Near-Infrared Emitting Polymer Nanogels for Efficient Sentinel Lymph Node Mapping

Young-Woock Noh,[†,⊥] Seong-Ho Kong,[‡,⊥] Doo-Yeol Choi,[§] Hye Sun Park,[†] Han-Kwang Yang,[‡] Hyuk-Joon Lee,[‡] Hee Chan Kim,[‡] Keon Wook Kang,[‡] Moon-Hee Sung,[§] and Yong Taik Lim[†,*]

[†]Graduate School and Department of Analytical Science and Technology, Chungnam National University, Daejeon 305-764, South Korea, [‡]Seoul National University College of Medicine, Seoul National University Hospital, 101 Daehang-Ro, Jongno-gu, 110-744, Seoul, South Korea, and [§]Kookmin University, 861-1 Chongnung-dong, Songbuk-gu, Seoul 136-702, Korea. [⊥]These authors contributed equally to this work.

ABSTRACT Sentinel lymph node (SLN) mapping has been widely used to predict the metastatic spread of primary tumor to regional lymph nodes in clinical practice. In this research, a new near-infrared (NIR)-emitting polymer nanogel (NIR-PNG) having a hydrodynamic diameter of about 30 nm, which is optimal for lymph node uptake, was developed. The NIR-emitting polymer nanoprobes were designed and synthesized by conjugating IRDye800 organic dye to biodegradable pullulan-cholesterol polymer nanogels. The NIR-PNG nanoprobes were found to be photostable compared with the IRDye800-free dye at room temperature. Upon intradermal injection of the NIR-PNG into the front paw of a mouse, the nanoprobes entered the lymphatic system and migrated to the axillary lymph node within 2 min. The NIR fluorescence signal intensity and retention time of NIR-PNG in the lymph node were superior to the corresponding properties of the IRDye800-free dye. A immunohistofluorescence study of the SLN resected under NIR imaging revealed that the NIR-PNG nanoprobes were predominantly co-localized with macrophages and dendritic cells. Intradermal injection of NIR-PNG nanoprobes into the thigh of a pig permitted real-time imaging of the lymphatic flow toward the SLN. The position of the SLN was identified within 1 min with the help of the NIR fluorescence images. Taken together, the experimental results demonstrating the enhanced photostability and retention time of the NIR-PNG provide strong evidence for the potential utility of these polymer probes in cancer surgery such as SLN mapping.

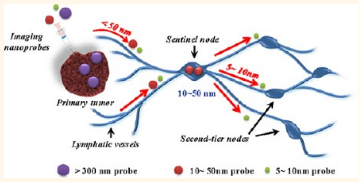

KEYWORDS: polymer nanogel · nanoprobe · sentinel lymph node · NIR optical imaging · cancer

The metastatic spread of primary cancers to regional lymph nodes is one of the most important prognostic factors determining the need for adjuvant chemotherapy. The sentinel lymph node (SLN) refers to the first regional lymph node to which cancer cells are most likely to spread from a primary tumor.[1−4] SLN biopsy procedures have been widely used to predict the status of a tumor in clinical practice. Dye-guided or radio-guided methods, or a combination of both, are currently used to map the SLN during the surgery.[5−7] Although the dye-guided method is technically easy, very safe, and cost-effective, dyes are not visible if the lymph node is located deep within the patient. Dye-guided methods also have a high rate of false-negative results because the small dye molecules can readily diffuse through the true SLN to the second- and third-tier nodes.[8] Although a lymph node in deep tissues can be detected by radio-guided methods (gamma detector), high radioactivity at the primary injection site could interfere with intraoperative lymph node detection of nearby lymph nodes.

For this reason, materials that emit fluorescence in the near-infrared (NIR) region are currently used for SLN mapping.[2,9−11] The NIR region of the spectrum, between 700 and 1000 nm, is advantageous for *in vivo* imaging because the autofluorescence background in this spectral range is low, optical scattering is low, and significant imaging depths are possible.[9,12] Recently, NIR fluorescence dyes, such as indocyanine green (ICG),[11,13,14] IRDye800,[15] and heptamethine cyanine dye IR-780 iodide,[16] have been used for *in vivo* imaging and SLN mapping in animal and clinical studies. ICG showed promise in SLN mapping applications for breast cancer and gastric cancer due to its biocompatibility;[17,18] however, ICG molecules readily diffuse through the true SLN and travel to other lymph nodes, similar to the blue dye, due to its low molecular weight.[19] Researchers have attempted to address these *in vivo* problems without altering the dye properties by encapsulating ICG in biodegradable polymers.[20,21] However, the molecular sizes of such polymers are in the upper limits of the preferred range for lymphatic uptake.[22,23] Although the magnitude of the

* Address correspondence to yongtaik@cnu.ac.kr.

Received for review May 3, 2012 and accepted August 4, 2012.

Published online August 04, 2012
10.1021/nn301949y

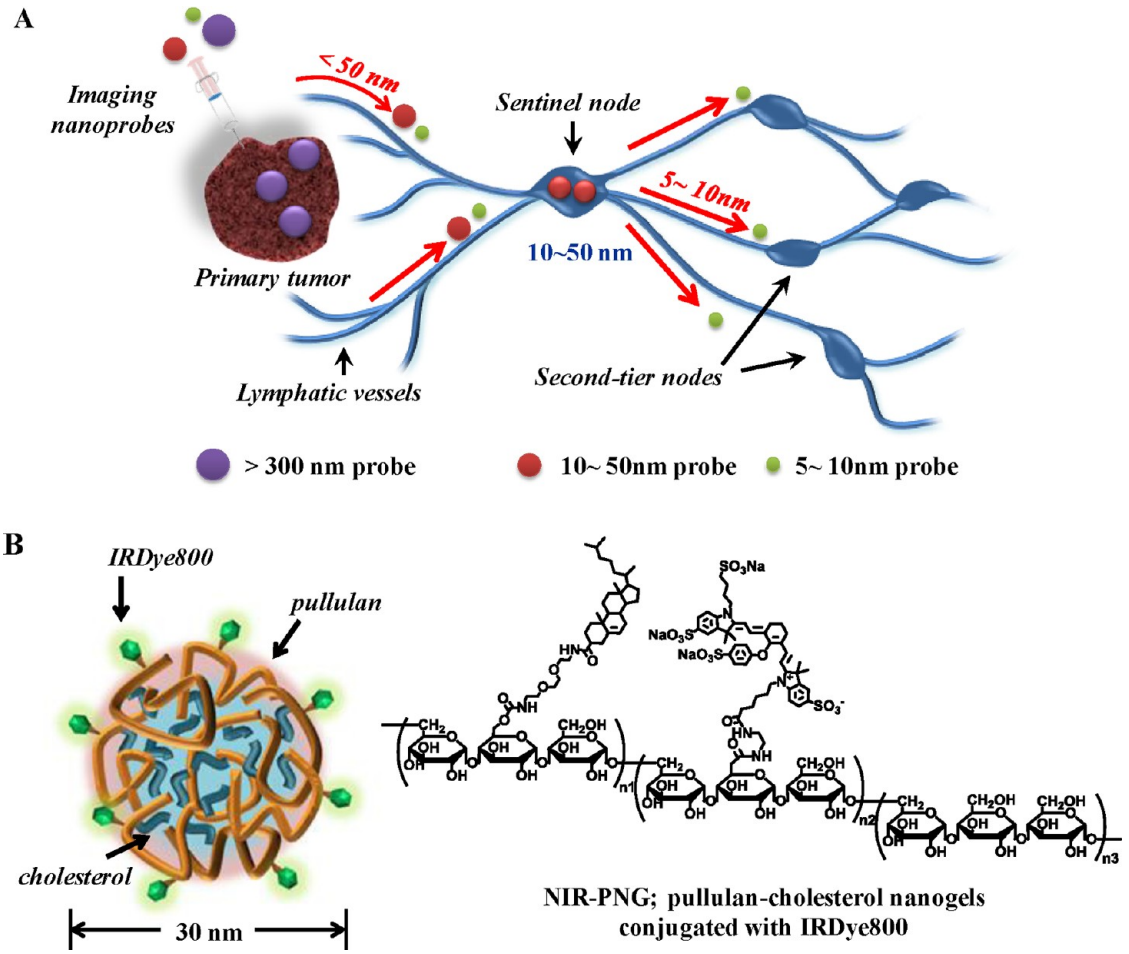

Figure 1. Schematic illustration of NIR-PNG nanoprobes optimized for SLN mapping. (A) Schematic illustration of SLN mapping using a nanoscale imaging probe. Imaging probes on the 5−10 nm size scale can flow through the SLN into adjacent nodes in the chain; nanoprobes >300 nm in size rarely leave the injection site. Nanoprobes with a hydrodynamic diameter of 10−50 nm exhibit rapid uptake into SLN and do not leave. (B) Chemical structure of NIR-PNG based on pullulan-cholesterol nanogels conjugated with IRDye800 organic dye.

optimal size is still under debate, it is generally accepted that nanoscale agents with hydrodynamic diameters of 10−50 nm exhibit rapid uptake into the lymphatic system and can be effectively used to identify the SLN. Nanoprobes with a hydrodynamic diameter < 5 nm partition into the bloodstream; nanoprobes on the 5−10 nm size scale can flow through the SLN into adjacent nodes in the chain; nanoprobes > 300 nm in size rarely leave the injection site (Figure 1A).[24] Recently, inorganic nanoscale (<20 nm) quantum dots have been considered to be promising nanoprobes for SLN mapping in living organisms;[2,3,24−26] however, practical applications of quantum dots are limited by their potential toxicity.[27,28] Here, we designed and synthesized a novel NIR-emitting polymer nanogel having an optimal size for SLN mapping, based on pullulan-cholesterol nanogels conjugated with IRDye800 organic dye. Pullulan, neutral linear polysaccharide, is produced from starch by *Aureobasidium pullulans* and has been extensively studied for applications in the biomedical field due to its water-soluble, biodegradable, nontoxic, and nonimmunogenic properties, as well as its amenability to chemical modification.[29−33] In this research, we designed a pullulan-based polymer nanogel by conjugating a hydrophobic moiety (cholesterol) to the hydrophilic pullulan backbone. The hydrophobic moiety, cholesterol, induced the pullulan-cholesterol copolymers to form a self-assembled nanogel structure under the balance of hydrophilic and hydrophobic forces. The size of the polymer nanogel was controlled for efficient SLN mapping, and IRDye800 was conjugated on the surface of the self-assembled nanogels. The potential of SLN mapping was evaluated by the size-controlled NIR-PNG nanoprobes in both small animals (mouse) and large animals (pigs).

RESULTS AND DISCUSSION

Synthesis of NIR-PNG Nanoprobes. Polymer modification for synthesis of NIR-emitting polymer nanogels was done in three steps (Figure S1): (i) pullulan-cholesterol conjugate was synthesized by conjugating amine-cholesterol on pullulan; (ii) amine moieties were additionally introduced for the conjugation of NIR-emitting

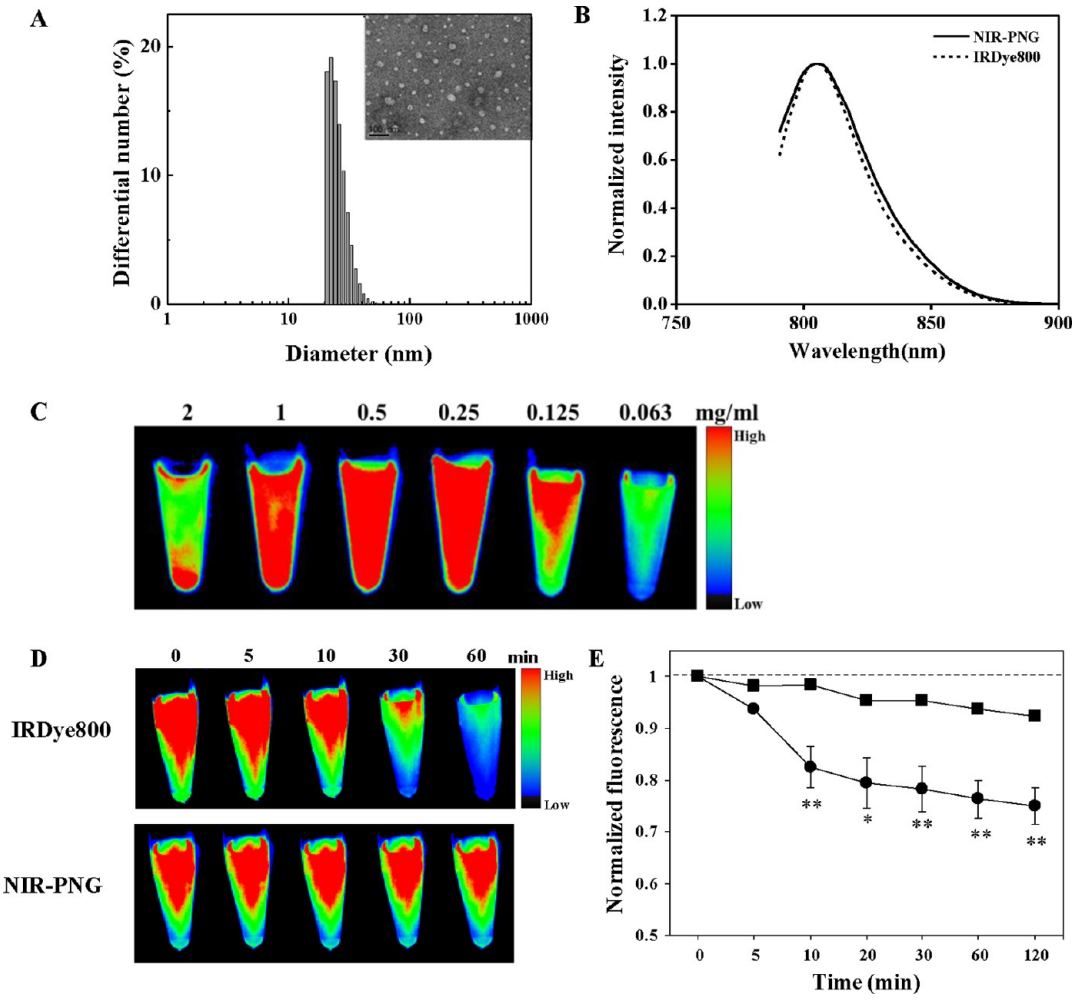

Figure 2. Physicochemical properties of NIR-PNG nanoprobes. (A) Size and size distribution of NIR-PNG nanoprobes measured by DLS and TEM (inset). The scale bar in the TEM image represents 100 nm. (B) Fluorescence spectra of NIR-PNG nanoprobes and IRDye800 dye. The spectra were normalized for the maximum fluorescence at 810 nm. (C) *In vitro* NIR fluorescence image (pseudocolor) of the NIR-PNG nanoprobes in water according to the concentration of NIR-PNG nanoprobes. (D, E) Fluorescence stability of IRDye800 dye (1 μg/mL) and NIR-PNG nanoprobes (100 μg/mL, conjugated with 1 μg/mL IRDye800) was determined by using the NIR fluorescence images (D) and fluorescence maximum emission spectra (E) in water at room temperature over time (2 h). Black squares indicate NIR-PNG nanoprobe, black circles indicated IRDye800. *$p < 0.05$, **$p < 0.01$ compared with NIR-PNG nanoprobes at the same times.

fluorophores; (iii) NHS-terminated IRDye800 was finally conjugated with aminated pullulan-cholesterol conjugate. Detailed information on the chemical scheme, synthesis, and characterization is shown in the Materials and Methods section and Supporting Information (Figures S1−S6). The PNG synthesized had a hydrodynamic diameter of about 30 nm (Figure 1B), which is considered optimal for lymph node uptake. The zeta potentials of the NIR-PNG nanoprobes were measured at each synthesis step (Table S1). Upon introduction of the amine, a remarkable increase in the zeta potential was observed, from -9.76 ± 2.29 to 34.76 ± 0.70 mV, indicating that the negatively charged surface was converted to a positively charged surface. IRDye800 introduction, however, led to a decrease in zeta potential (11.05 ± 0.35 mV) due to the attachment of the negatively charged IRDye800 dye to the nanogel surface (Table S1). Measurement of the amount of dye per milligram of NIR-PNG nanoprobes revealed that 1 mg of NIR-PNG nanoprobes conjugated approximately 10 μg of IRDye800. The size of the NIR-PNG nanoprobes was measured by dynamic light scattering (DLS), which revealed that the mean diameter was approximately 30 nm (Figure 2A). In addition, we also measured the average sizes and distributions of these nanoprobes ($n = 134$) using TEM. The size was found to be slightly smaller than those measured by DLS. The possible reason may be that the TEM images were obtained after the air-drying process, which causes the nanoprobes to shrink and attain a smaller size than under water. It is well known that the particle size of a tracer exhibits a strong impact on the migration time during SLN mapping and the optimal tracer size for lymph node uptake is in the range 10−50 nm.[3,22,23] Particles smaller than 5 nm may diffuse through the lymph node and enter the bloodstream directly, whereas larger

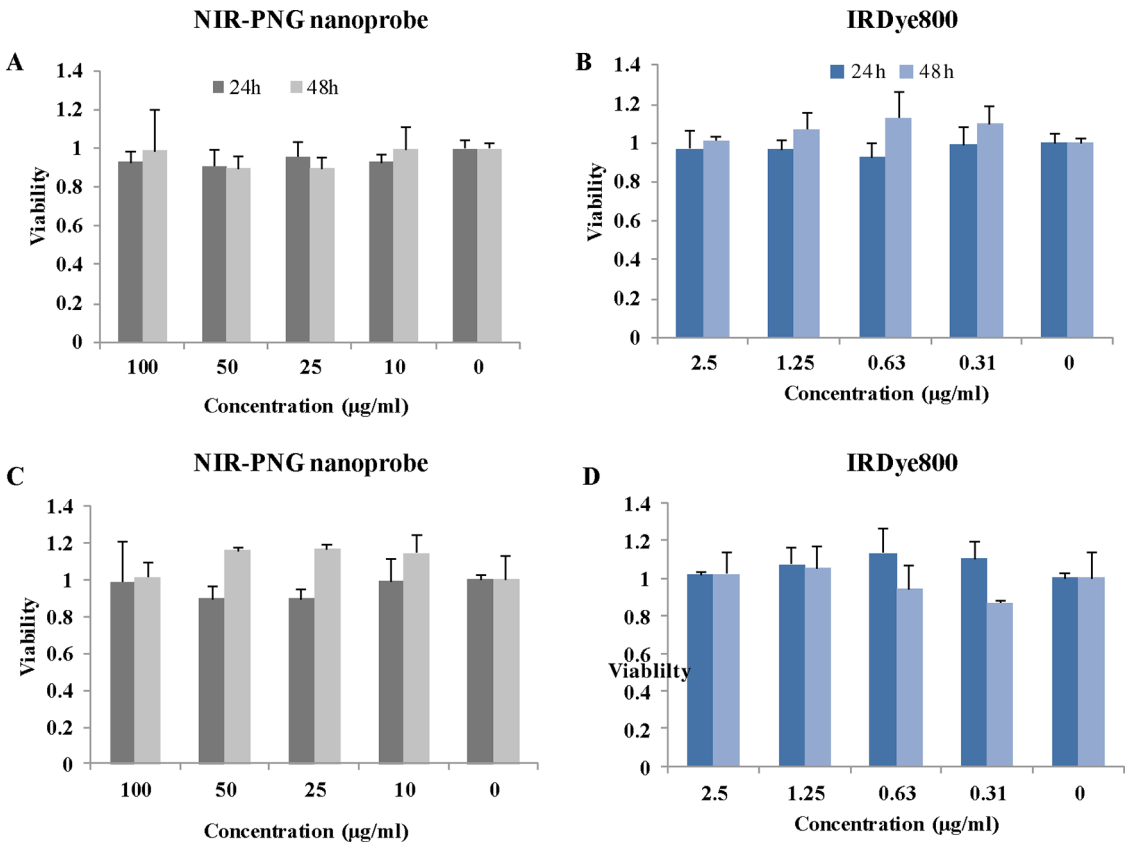

Figure 3. Cytotoxicity of the NIR-PNG nanoprobes. Cytotoxicities of the NIR-PNG nanoprobes (A and C) and IRDye800 (B and D) were determined for mouse DC2.4 cells (A and B) and CT-26 adenocarcinoma (C and D) after 24 and 48 h of incubation for each molecule at indicated concentrations.

particles cannot enter the endothelial cell junctions and may be retained for long periods at the site of injection (Figure 1A).[3] Taken together, the experimental results demonstrated that the NIR-PNG nanoprobes can be used as efficient molecular imaging probes for SLN mapping that can be rapidly transported to and retained in the SLN.

Optical Properties of NIR-PNG Nanoprobes. The emission spectrum of NIR-PNG nanoprobes was compared to the spectrum of IRDye800-free dye dissolved in water at 25 °C. As shown in Figure 2B, the emission spectra of the IRDye800 and NIR-PNG nanoprobes agreed well in water at 25 °C, and no spectral shifts were observed in the emission spectrum of the NIR-PNG nanoprobes (Figure 2B). These results suggested that NIR-PNG nanoprobes did not influence the emission spectrum of IRDye800 at room temperature. NIR fluorescence imaging was performed on serial dilutions (63 to 2000 μg/mL) of the NIR-PNG nanoprobes using a 785 nm LED light source and an 835/45 nm emission filter. The NIR fluorescence intensity was dependent on the concentration of the NIR-PNG nanoprobes. The fluorescence intensity was highest at the NIR-PNG nanoprobes concentration of 0.5 mg/mL, and as the concentration was increased up to 1−2 mg/mL, the fluorescence signal decreased (Figure 2C). In general, the fluorescence intensity of dye solutions increases as the concentration of the dye increases; however, at a certain threshold concentration, the fluorescence intensity begins to decrease because the emitted photons are reabsorbed by other fluorescent dyes in the solution.[34] When the fluorescence intensities of IRDye800 and NIR-PNG nanoprobes were measured in water for 2 h at 25 °C, the fluorescence intensity of IRDye800 decreased over 2 h at 25 °C (Figure 2D, E). In fact, the long-term stability of IRDye800 dye in an aqueous solution has been found to be undesirable during its development for clinical applications, although IRDye800 is more stable in an aqueous solution than conventional cyanine NIR dye. In contrast, the fluorescence intensity of the NIR-PNG nanoprobes did not decrease significantly over time relative to the IRDye800 at 25 °C (Figure 2D, E). These data demonstrated that the photostability of IRDye800 could be enhanced after conjugation on the surface of the polymer nanogel.

Cytotoxicity of NIR-PNG Nanoprobes. One of the stringent requirements for *in vivo* tracer applications is low cytotoxicity. Cytotoxicity studies of the NIR-PNG nanoprobes were conducted using a dendritic cell line (DC2.4) and an epithelial colorectal adenoma cell line (CT-26) to measure the cell viability after incubation with NIR-PNG nanoprobes or IRDye800. The dendritic cell line was especially chosen as a model cell line for viability study because these cells are typical dendritic cells present in lymph nodes. As shown in Figure 3, the

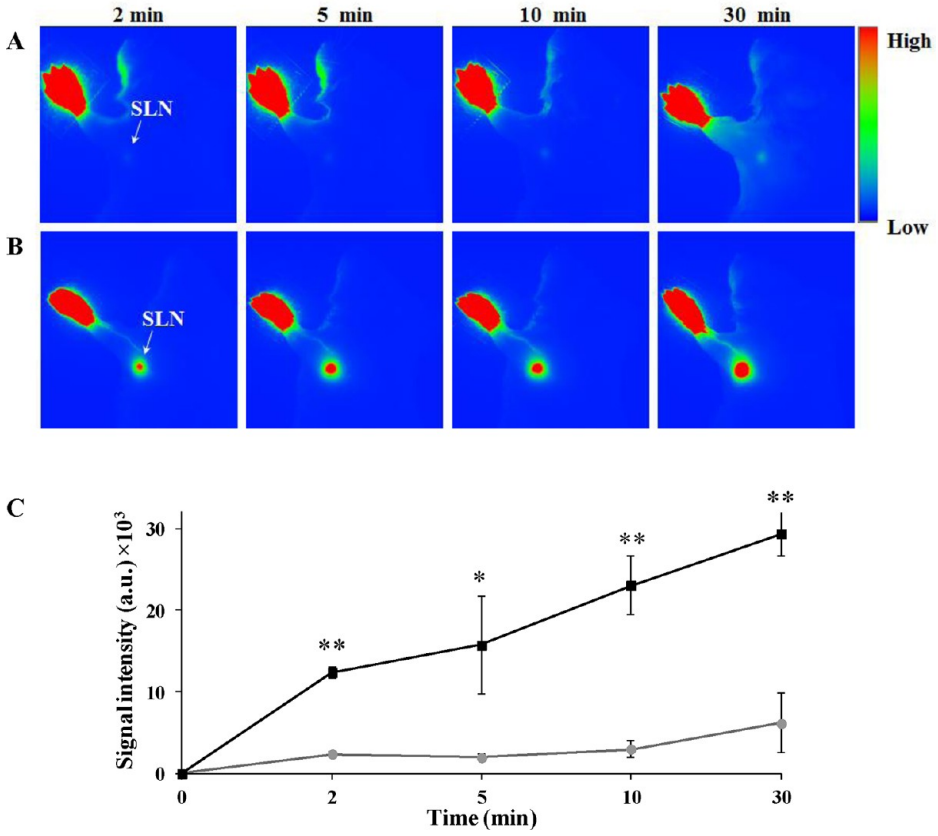

Figure 4. *In vivo* **SLN imaging in a small animal.** *In vivo* **NIR fluorescence images (pseudocolor) at indicated time after intradermal injection into the right paw of a mouse with IRDye800 (A) and NIR-PNG nanoprobes (B). The arrows indicate the axillary sentinel lymph node. (C) Signal intensity of sentinel lymph node is plotted** *versus* **time in IRDye800-injected (gray circles) and NIR-PNG nanoprobes-injected (black squares) mice. a.u.: arbitrary units. *$p < 0.05$, **$p < 0.01$ compared with IRDye800 at same times.**

NIR-PNG nanoprobes generally showed no cytotoxic effects toward both the DC2.4 (Figure 3A) and CT-26 cell line (Figure 3B) up to 100 μg/mL and higher concentrations (Figure S7). The results suggest that the cytotoxicity of NIR-PNG nanoprobes was negligible and could be used for *in vivo* applications. To determine whether NIR-PNG nanoprobes have any effect on cytokine production of DC2.4 cells, we measured the levels of IL-6 and TNF-α after incubation with NIR-PNG nanoprobes or IRDye800 for 24 h. As shown in Figure S8, the presence of nanoprobes did not alter cytokine levels, whereas dendritic cells (DCs) responded to LPS stimulation with a strong increase in cytokine production. In this analysis, we found that NIR-PNG nanoprobes did not affect production of the immune response-associated cytokines.

***In Vivo* SLN Mapping in a Small Animal.** After demonstrating enhanced photostability and nontoxicity of the NIR-PNG nanoprobes, we evaluated them for use as a SLN mapping agent in mice. For this purpose, the NIR-PNG nanoprobes (50 μg of samples in 50 μL of water) were intradermally injected into the right paw of a mouse and imaged for *in vivo* migration of NIR-PNG nanoprobes using a NIR optical imaging system. Weak signal of IRDye800 was detected in axillary LN of mice injected with only free IRDye800 into the paw, because due to its small size, injection of free IRDye800 into the mouse paw resulted in the easy passage of the dye through the SLN and diffusion into other lymph nodes (Figure 4A).[24] In contrast, the SLN and lymphatic vessels (LV) of the mice injected with NIR-PNG nanoprobes were visualized from 2 min to more than 30 min (Figure 4B), and the NIR fluorescence signal of the SLN was much brighter compared to the signal of the IRDye800, over 2−30 min (Figure 4C). Methylene blue dye has been used as a safe and effective substitute for isosulfan blue dye to identify the SLN in animals and patients.[35] After injection of methylene blue dye at the same site, followed by removal of the skin, the area that generated strong NIR fluorescence signals was confirmed to be a SLN ($n = 3$, Figure 5A, B; IRDye800, 5E, F; NIR-PNG) after 30 min postinjection. These findings were further corroborated by *ex vivo* imaging of excised lymph nodes. The NIR fluorescence signals associated with the SLN, but not the adjacent fat tissue, indicated preferential accumulation of the NIR-PNG nanoprobes in the SLN. The NIR-PNG nanoprobes were accumulated in the SLN to a greater extent than IRDye800 (Figure 5C, D; IRDye800, 5G, H; NIR-PNG). The lymph node retention time of the NIR-PNG

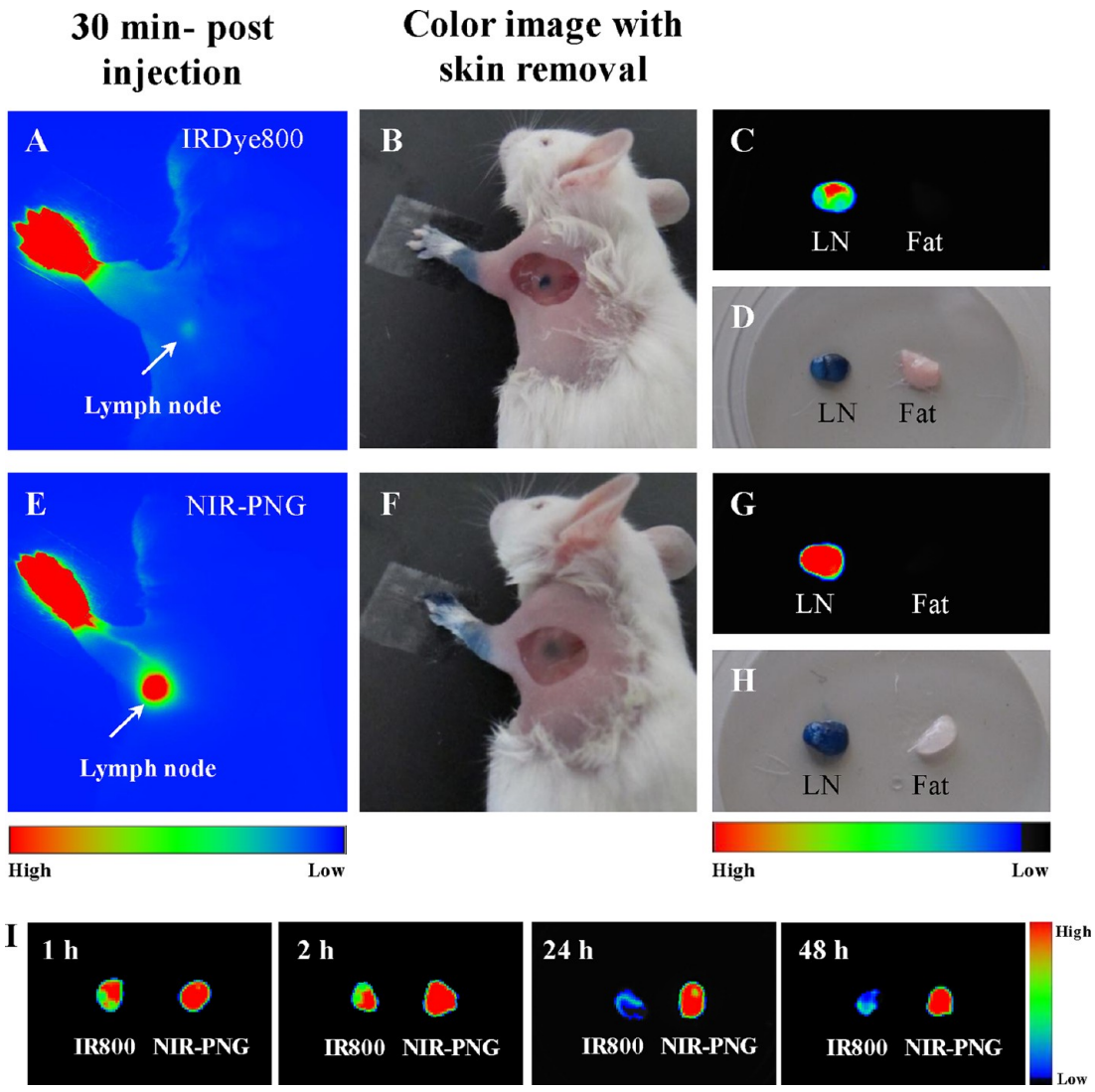

Figure 5. SLN mapping procedure with IRDye800 and NIR-PNG nanoprobes. (A, E) *In vivo* NIR fluorescence images (pseudocolor) at 30 min postinjection of the IRDye800 dye (0.5 μg in 50 μg of PBS) (A) and NIR-PNG nanoprobes (50 μg, conjugated with 0.5 μg of IRDye800, in 50 μg of PBS) (E). The arrows indicate the axillary SLN. (B, F) Color images of a mouse after methylene blue dye injection and skin removal after an injection of the IRDye800 (B) and NIR-PNG nanoprobes (F). (C−H) *Ex vivo* NIR fluorescence (C, G) and color (D, H) images of dissected LN and fat tissue of a mouse injected with the IRDye800 (C, D) and NIR-PNG nanoprobes (G, H). (I) *Ex vivo* NIR fluorescence images of dissected SLN on time points in the range 1−48 h postinjection.

nanoprobes and IRDye800 was measured at 1−48 h postinjection (Figure 5I). The *ex vivo* NIR fluorescence of NIR-PNG nanoprobes was much brighter than that of IRDye800 at 1−48 h postinjection. The NIR-PNG nanoprobes were present at qualitatively consistent levels in the lymph node even at 24 and 48 h postinjection, whereas the IRDye800 was not visibly present in the lymph nodes at these time points (Figure 5I). These data demonstrated that the NIR-PNG nanoprobes acted as a good tracer for SLN mapping, and the mouse data are relevant to axillary SLN mapping for breast cancer.

Localization of NIR-PNG Nanoprobes within the SLN. The study was further extended by performing immunohistofluorescence of SLN dissected from mice that had been injected with the NIR-PNG nanoprobes or IRDye800 after 30 min. As shown in Figure 6, the immunohistofluorescence image of the SLN indicated good regional lymph node retention of the NIR-PNG nanoprobes at 30 min, whereas only a fraction of the IRDye800 was localized in the lymph node. The localization and retention characteristics of the NIR-PNG nanoprobes within the lymph node were investigated. T cells tend to localize in the central region of the lymph node, whereas B cells are often found at germinal centers located toward the outer membrane. The other major cell types present in lymph nodes are dendritic cells and macrophages, and their locations are dispersed throughout the subcapsular space.[22] The IRDye800 was not localized in the subcapsular space with the macrophages ($CD68^+$ cell) (Figure 6A, C) or DCs ($CD205^+$ cell) (Figure 6E). However, NIR-PNG

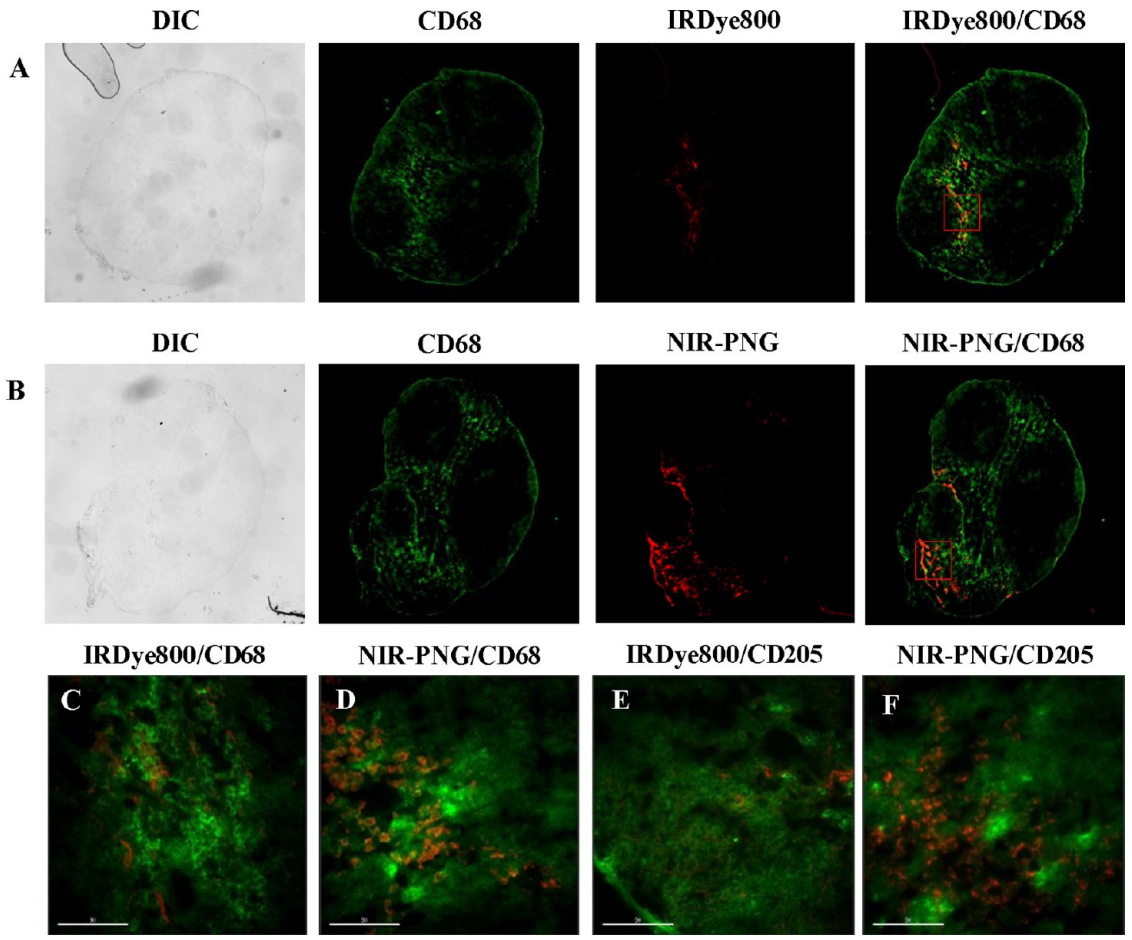

Figure 6. Immunohistofluorescence analysis of the SLN. Immunohistofluorescence analysis of the dissected SLN of a mouse injected with the IRDye800 dye (A, C, E) or NIR-PNG nanoprobes (B, D, F). The slides were stained with anti-CD68 (F4/80, macrophage, A–D) or anti-CD205 (DEC-205, dendritic cell, E, F). (C, D) Enlarged images of red squares. DIC, differential interference contrast; green, CD68 and CD205; red, IRDye800 and NIR-PNG (pseudocolor). Scale bars represent 90 μm.

nanoprobes were significantly co-localized with macrophages (Figure 6B, D) or DCs (Figure 6F). As shown in enlarged images in Figure S5, the fluorescence signals from the IRDye800 were exhibited outside the cells (Figure 6A, C and Figure S9A, arrowhead). In contrast, many fluorescence signals from the NIR-PNG nanoprobes were exhibited on the cell surface and inside the cells (Figure 6B, D and Figure S9B, arrow). These data reveal that the NIR-PNG nanoprobes delivered to the SLN were primarily phagocytosed by phagocytic cells such as macrophages and dendritic cells, whereas little IRDye800 could be phagocytosed in phagocytic cells. These results also suggested that NIR-PNG nanoprobes accumulated effectively in the lymph nodes. *In vitro* cellular uptake was evaluated by incubating a murine dendritic cell line (DC2.4) with NIR-PNG nanoprobes and IRDye800 to confirm their *in vivo* action. Fluorescence microscope and flow cytometric analysis data reveal that the NIR-PNG nanoprobes were more efficiently taken up by DC2.4 cells than IRDye800 (Figure 7A, B and Figure S10). To further determine the intracellular localization of NIR-PNG nanoprobes in DC2.4 cells, lysosomes were stained with a FITC-labeled lysosome-specific antibody (FITC-LAMP-1 antibody) and LysoTracker. Internalized NIR-PNG nanoprobes were mainly co-localized with the lysosomes of the cells (Figure 7C and Figure S11), indicating that internalized NIR-PNG nanoprobes preferentially localized in the lysosomal compartments of phagocytic cells.

***In Vivo* SLN Imaging in a Large Animal.** After getting promising results in small animals, we further investigated the use of NIR-PNG nanoprobes in large animal systems comparable to humans in size. Intradermal injection of NIR-PNG nanoprobes (100 μg in 100 μL of water) into the thigh of a 35 kg pig ($n = 5$) permitted the real-time imaging of the lymphatic flow toward the SLN (see the video provided in the Supporting Information). The surgeon was quickly able to identify the position of the SLN with the help of the NIR fluorescence images. Interestingly, the NIR fluorescence images showed that the lymphatic channels diverged from the injection site, then coalesced into the SLN (Figure 8A, B). The surgeon could identify the SLN within 1 min, and the NIR fluorescence intensity of the SLN increased dramatically upon dissection of the tissue (8 min after injection, Figure 8C). Histofluorescence analysis of the resected

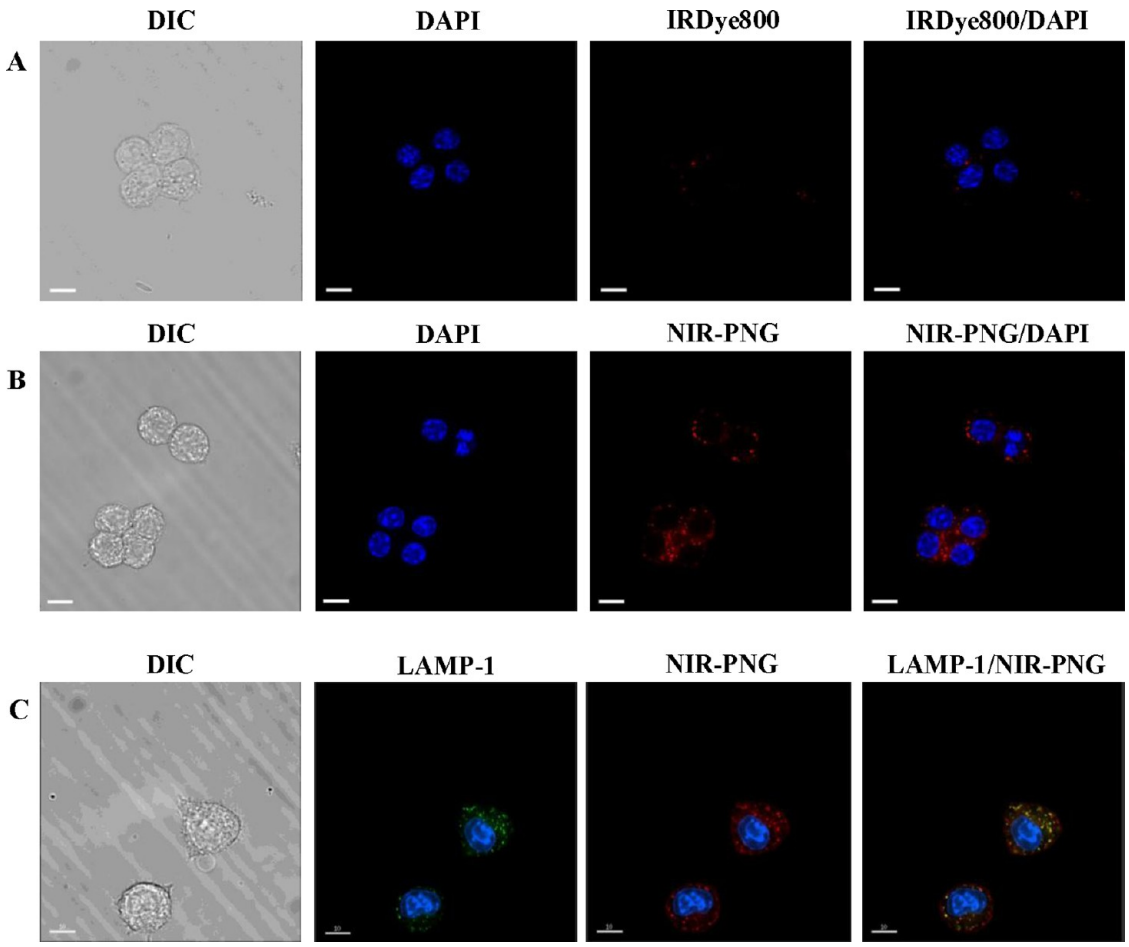

Figure 7. *In vitro* **fluorescence images of NIR-PNG nanoprobes accumulated in the cell. Fluorescence microscopy images of DC2.4 cells treated with 2.5 μg/mL IRDye800 dye (A) and 0.1 mg/mL NIR-PNG nanoprobes (B). The NIR fluorescence images (red, pseudocolor) were obtained by using excitation (740/35 nm) and emission (780LP nm) filters. (C) DC2.4 cells, treated with NIR-PNG nanoprobes, were stained with FITC-conjugated LAMP-1 monoclonal antibody (green). Localization of lysosomes (green) and NIR-PNG nanoprobes (red, pseudocolor) was determined by fluorescence microscopy. Scale bars represent 10 μm; DIC, differential interference contrast.**

tissue showed that the NIR-PNG nanoprobes were completely trapped in the SLN and confined to the outermost rim of the node (Figure 8D, E). Both the NIR histofluorescence image and enlarged image (Figure 8F, G) showed that the NIR-PNG nanoprobes were accumulated in the SLN, taken up by lymph node cells, and subsequently localized in the cell interior.[22] These data are consistent with the well-known sieving properties of the subcapsular sinus in lymph node.

CONCLUSION

We have successfully synthesized NIR-PNG nanoprobes using self-assembled pullulan-cholesterol nanogels conjugated with IRDye800 and demonstrated their use as an efficient SLN mapping agent. The combination of NIR fluorescence dye and a nanosize polymer nanogel (PNG) dramatically improved the photostability and retention time of the NIR fluorophore under physiological conditions in the SLN. The NIR-PNG nanoprobes also displayed a bright fluorescent signal both in the SLN and in the lymphatic vessels. To the best of our knowledge, this study provides the first demonstration of SLN mapping using NIR-PNG nanoprobes in both small and large animal models. The NIR-PNG nanoprobes are expected to be used as excellent imaging contrast agents for SLN mapping in human clinical models.

MATERIALS AND METHODS

Materials. Pullulan was purchased from Wako Pure Chemicals (Tokyo, Japan). Cholesteryl chloroformate (97%), 1,1′-carbonyldiimidazole, 2,2′-(ethylenedioxy) bis(ethylamine) (EDBE), 1,2-ethanediamine (EDA), and methylene blue dye at a 1% concentration were purchased from Sigma-Aldrich (St. Louis, MO, USA). IRDye800 and IRDye800 NHS ester were purchased from Li-COR (Lincoln, NE, USA). The dyes were resuspended to a concentration of 30 mM in DMSO (Li-COR) under reduced light conditions and stored at −80 °C.

Synthesis of Pullulan-Cholesterol Nanogels. The structure and reaction scheme of pullulan-cholesterol nanogels are presented in Figures S1−S3. Cholesteryl chloroformate (2.25 g, 5 mmol)

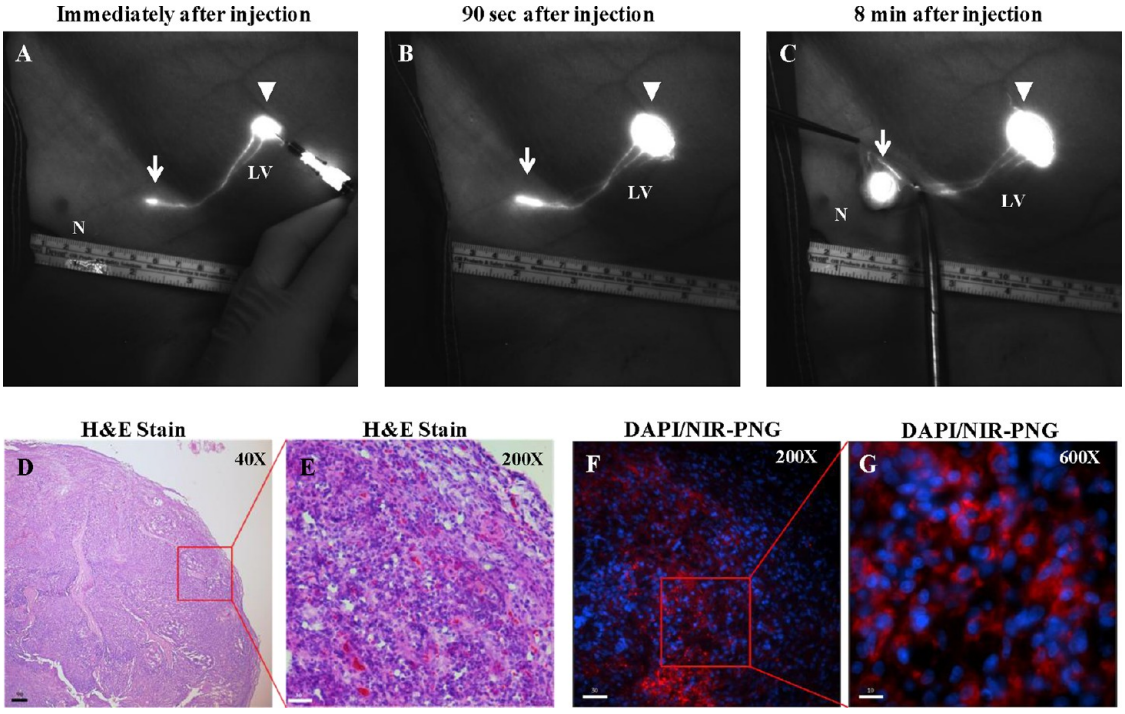

Figure 8. *In vivo* **SLN mapping in a large animal. (A−C) NIR-PNG nanoprobes were injected (arrowhead) into the pig thigh, and lymphatic flow was mapped in real time to the SLN (arrows). Shown are the NIR fluorescence images immediately after injection (A), 90 s postinjection (B), and 8 min postinjection with skin stripping (C). The fluorescence images were obtained using an intraoperative NIR fluorescence imaging system consisting of a 785 nm diode laser (excitation), an 835/45 nm emission filter (emission), and a CCD camera; 100 ms exposure time. N, nipple; LV, lymphatic vessels. (D−G) Histologic analysis of frozen sections of the SLN. Shown are the images of the hematoxylin and eosin (H&E) stained section (D, E) and the fluorescence image of a section stained with DAPI (F, G). (D) Original magnification (40×); scale bar represents 90 μm. (E) enlarged image (200×) of the red square region in (D); scale bar represents 30 μm. (F) Fluorescence image (200×) of (E); scale bar represents 30 μm. (G) Enlarged image (600×) of the red square region in (F); scale bar represents 10 μm.**

was added to a solution of 2,2′-(ethylenedioxy) bis(ethylamine) (37 g, 250 mmol) in dry toluene (250 mL) over an ice bath. The reaction mixture was stirred at room temperature overnight, washed with water, dried over anhydrous magnesium sulfate, and evaporated in a rotary evaporator. The residue was dissolved in dichloromethane (20 mL), and methanol (20 mL) was added to it. The resulting suspension was filtered to remove the biscarbamate, and the filtrate was evaporated in a rotary evaporator to give a white solid. The ethylenediamine-pullulan-2,2′-(ethylenedioxy)-bis(ethylamine)cholesterol conjugate (pullulan-cholesterol) was successfully synthesized by esterification of the hydroxyl group of pullulan and the amine group of the cholesterol-2,2′-(ethylenedioxy) bis(ethylamine) conjugates (cholesterol-amine) along with ethylene diamine. To synthesize pullulan-cholesterol, 1 g of pullulan and 0.086 g of cholesterol-amine were reacted in DMSO in the presence of 1,1′-carbonyldiimidazole (1.134 g). The ^{1}H NMR spectrum was used to quantify the reaction between pullulan and cholesterol-amine. The ^{1}H NMR spectra of cholesterol-amine and pullulan-cholesterol are shown in Figures S2 and S3. The proton peak of the cholesterol methyl group (0.9−1.2 ppm) was observed in the ^{1}H NMR spectrum of pullulan-cholesterol, and the hydroxyl peak of dextrose appeared at 4.8−5.2 ppm (Figures S2 and S3). After grafting the cholesterol-amine onto pullulan, the graft ratio of cholesterol to the synthesized pullulan-cholesterol conjugate was 1.7%. Then, the pullulan-cholesterol conjugate was aminated with ethylenediamine in DMSO. For amination, pullulan-cholesterol (150 mg) and ethylenediamine (150 mg) were mixed in DMSO (50 mL) containing 1,1′-carbonyldiimidazole (38 mg) for 24 h. The amine-pullulan-cholesterol was quantified by elemental analysis to determine the ratio of C, N, and H. The percentage of carbon present in the sample did not change significantly (pullulan-cholesterol: 41%; amine-pullulan-cholesterol: 40%), but the percentage of nitrogen changed dramatically (pullulan-cholesterol: 0.09%; amine-pullulan-cholesterol: 1.5%). Carbon was the dominant element in the dextrose of pullulan, and nitrogen was present in the cholesterol linker and in the aminated ethylene diamine. The percentage of C was derived from the molecular mass of dextrose, 162 amu, and the percentage of N was derived from the molecular mass of ethylenediamine-*N*,*N*, 28 amu, yielding a 6.68% synthetic yield. The synthesized pullulan-cholesterol and amine-pullulan-cholesterol were easily self-assembled to form micelles in aqueous medium (Figure S4).

Preparation and Characterization of the NIR-PNG Nanoprobes. For the fabrication of the NIR-PNG nanoprobes, 2 mg/mL amine-pullulan-cholesterol solutions were mixed with IRDye800 NHS ester (50 μg/mg) dissolved in DMSO. The conjugation reaction proceeded for 2 h at room temperature. NIR-PNG nanoprobes were separated using Bio-Spin columns filled with Bio-Gel P-6 gels (Bio-Rad Laboratories, Richmond, CA, USA) (Figures S5 and S6). The amount of conjugated dye was estimated to be 10 μg of dye per 1 mg of NIR-PNG nanoprobes *via* UV−vis spectrophotometer (NEOSYS-2000, Sinco, Seoul, Korea). The fluorescence spectra were measured by a fluorescence spectrophotometer (LS 55, PerkinElmer Instruments, Wellesley, MA, USA) using an excitation wavelength of 775 nm and an emission range of 780−900 nm. The spectra were normalized relative to the maximum fluorescence (λ_{em} = 810 nm) of IRDye800. To obtain the quantum yield of the IRdye800 and NIR-PNG dispersed in aqueous solutions, UV−vis absorption and fluorescence spectra were measured. UV−vis absorption spectra were recorded on a Jenway (Genova, Dunmow, UK) spectrophotometer. Diluted solutions of the IRdye800 and NIR-PNG were placed in a 1 cm quartz cuvette, and their absorption and corresponding fluorescence spectra were measured. The photoluminescence spectra were recorded on a spectrometer (Acton 2300i, Acton, MA, USA). The room-temperature quantum yields were determined by comparing these samples with a standard reference organic dye, namely, rhodamine 6G, in

water with a quantum yield of 95%. The quantum yields of IRdye800 and NIR-PNG were 13.5% and 11.8%, respectively, similar to values reported in previous research.[15] The microstructures of the NIR-PNG nanoprobes were characterized using high-resolution transmission electron microscopy (HRTEM, JEM-3011, JEOL, Tokyo, Japan). The size distribution of the NIR-PNG nanoprobes was analyzed using dynamic light scattering technique with an electrophoretic light scattering photometer (ELS-Z, Otsuka Electronics, Osaka, Japan). The surface charge of the nanoprobes was determined by zeta potential measurements using an ELS-Z. NIR fluorescence imaging of the NIR-PNG nanoprobes was performed using an imaging system consisting of an excitation light source (785 nm, 500 mW diode laser) and a cold charge-coupled device (CCD) camera (Orca ERG; Hamamatsu Photonics, Hamamatsu City, Japan) with an emission filter (835/45 nm band-pass filter), designed and built in our laboratory.

Stability of the NIR-PNG Nanoprobes. The fluorescence stability of IRDye800 (1 μg/mL) and the NIR-PNG nanoprobes (100 μg/mL) was determined over 2 h using a fluorescence spectrophotometer. The aqueous solutions were prepared and placed in the dark at 25 °C. The fluorescence emission spectra were measured at an excitation wavelength of 775 nm. The maximum fluorescence (λ_{em} = 810 nm) intensity of each sample at a given time was normalized by the corresponding fluorescence emission at time zero. The average normalized fluorescence intensities for each triplicate experiment were plotted as a function of time. The fluorescence stability was determined from the NIR fluorescence images of IRDye800 (1 μg/mL) and the NIR-PNG nanoprobes (100 μg/mL) using an NIR imaging system, as described above. The aqueous samples were kept in the dark for 1 h at 25 °C and then transferred to a 0.2 mL tube. NIR fluorescence images of the samples were acquired using a 785 nm excitation light source and an 835/45 nm band-pass emission filter (0.02 s exposure time) at various time points over 1 h.

***In Vitro* Cytotoxicity Assay.** Cell cytotoxicity was measured by analyzing the cleavage of thiazoyl blue tetrazolium bromide (MTT; Sigma-Aldrich) by the succinate dehydrogenases of living cells to yield formazan. DC2.4 cells (2×10^4 cells/well) residing in the lymph nodes or the CT-26 (2×10^4 cells/well) murine epithelial colorectal adenoma cell line was seeded on a flat-bottomed 96-well plate (Corning Costar, Cambridge, MA, USA) in RPMI medium (Invitrogen, Grand Island, NY, USA) supplemented with 10% heat-inactivated fetal bovine serum (Invitrogen), 5×10^{-5} M 2-mercaptoethanol (Sigma-Aldrich), 50 IU/mL penicillin, and 50 mg/mL streptomycin (Invitrogen). After incubating the cells with various concentrations of the NIR-PNG nanoprobes and IRDye800 for 24−48 h, MTT (10 μL/well of a 5 mg/mL MTT stock solution in PBS) was directly added to each well, and the plates were incubated at 37 °C for 4 h. A colorimetric MTT assay was conducted by adding dimethyl sulfoxide (DMSO; Sigma-Aldrich) to solubilize the formazan, and the absorbance was measured at 562 nm.

***In Vitro* Fluorescence Microscopic Imaging.** The intracellular labeling capacity of the NIR-PNG nanoprobes was determined by incubating DC2.4 cells with 0.1 mg/mL NIR-PNG nanoprobes or 2.5 μg/mL IRDye800 in μ-slide eight-well microscopy chamber slides (ibidi Integrated Biodiagnostics, Munich, Germany) at a density of 2×10^4 cells per well for 24 h at 37 °C. After washing, the cells were fixed with 4% paraformaldehyde for 20 min at room temperature. After washing with PBS, the cells were mixed with 4,6-diamidino-2-phenylindole dihydrochloride (DAPI; Sigma-Aldrich) in PBS for 10 min. Fluorescence images were obtained using a DeltaVision PD Restoration Microscope System. The intracellular localizations of the NIR-PNG nanoprobes were analyzed by staining the DC2.4 cells with the lysosomal marker lysosome-associated membrane glycoprotein-1 (LAMP-1). The cells were washed three times and then fixed by adding 200 μL/well Cytofix/Cytoperm solution (BD PharMingen, San Diego, CA, USA) and incubating for 20 min. Cells were washed with phosphate buffered saline (PBS), blocked with 1% bovine serum albumin (BSA; Sigma) in PBS for 30 min at room temperature, and then incubated with FITC-conjugated anti-LAMP-1 monoclonal antibody (1D4B) (BD PharMingen) for 30 min at room temperature. After washing, the cells were examined using a DeltaVision PD Restoration Microscope System, as described above.

Animals. Female Balb/C mice aged 5 to 6 weeks (KOATECH, Pyeongtaek, Korea) were maintained under specific pathogen-free conditions, and female Yorkshire pigs weighing 35 kg (age: 11 weeks) were maintained under pathogen-free conditions. All experiments employing mice were performed in accordance with the Korean NIH guidelines for the care and use of laboratory research animals.

***In Vivo* SLN Mapping in a Small Animal.** For *in vivo* experiments, the BALB/c mice were anesthetized with 300 μL of a 2.5% avertin solution (2,2,2-tribromoethanol-*tert*-amyl alcohol, Sigma), and the imaging areas were treated with a depilatory cream. Thereafter, the NIR-PNG nanoprobes (50 μg in 50 μL of water) or IRDye800 (0.5 μg in 50 μL of water) was intradermally injected into the forepaw pad. Two minutes after injection, the mice were placed in a light-sealed area connected to the CCD camera, and NIR images (0.02 s exposure) of the axillary lymph nodes were acquired using a 785 nm, 500 mW diode laser as an excitation light source and an 835/45 nm band-pass emission filter. The laser illumination intensity was approximately 27.6 mW/cm^2. All images were processed using the Simple PCI software (Compix Inc., Cranberry Township, PA, USA). Methylene blue dye at a concentration of 1% was then reinjected at the same site to confirm the presence of the lymph node detected by the NIR image. After skin removal, photographs of the lymph node were obtained using a Canon digital camera. The kinetics of the NIR-PNG nanoprobes accumulation and retention in the lymph nodes were analyzed by dissecting the axillary LN after injection of 1.25 μg (in 50 μL of water) of IRDye800 and the 50 μg (in 50 μL of water) of NIR-PNG nanoprobes. Fluorescence images were obtained using an imaging system, as described above. The measurements were performed at 1, 2, 24, and 48 h after injection. Two mice were used in one experiment for SLN mapping, and the experiment was repeated three times (n = 6).

***In Situ* Histofluorescence.** The *in situ* distribution of the NIR-PNG nanoprobes was analyzed by dissecting the axillary LN 30 min after injection of 50 μg of NIR-PNG nanoprobes or 1.25 μg of IRDye800 and embedding in Tissue-Tek OCT compound (SAKURA, Tokyo, Japan) followed by freezing in liquid nitrogen. Cryosections (8 μm) were cut using a Tissue-Tek Cryo3Microtome/Cryostat (SAKURA) and transferred to glass slides. The sections were fixed with cold acetone for 5 min, dried, and frozen at −20 °C until use. The slides were washed in PBS and blocked with PBS containing 1% BSA for 1 h at room temperature. After an additional series of washes, the slides were stained with rat anti-mouse CD68 (F4/80, Serotec, Oxford, UK) and rat anti-mouse CD205 (DEC-205, Serotec) overnight at 4 °C to label the macrophages and dendritic cells, respectively. The slides were then stained with FITC-conjugated anti-rat IgG secondary antibodies (BD PharMingen, San Diego, CA, USA) for 1 h at room temperature. The slides were washed twice with PBS and then treated with DAPI in PBS for 10 min. After the final washing, the slides were mounted in 50% glycerol (in PBS) and examined by a fluorescence microscope (Olympus IX71, Olympus Optical, Tokyo, Japan) and a DeltaVision PD Restoration Microscope System (Applied Precision Technologies, Issaquah, WA, USA).

***In Vivo* SLN Mapping in a Large Animal.** For *in vivo* SLN imaging in large animal, pigs (n = 5) were anesthetized with intramuscular tiletamine-zolazepam (Zoletil, 12.5 mg/kg) and xylazine (Rompun, 2.33 mg/kg), intubated endotracheally, ventilated with 100% oxygen, and maintained with 1.5% to 2% isoflurane. Continuous oxygen saturation and heart rate were monitored throughout the experiment. NIR-PNG nanoprobes (100 μg in 100 μL of water) was injected intradermally into the thigh. After the injection, real-time images of the lymphatic flow toward the inguinal lymph node were acquired using the intraoperative NIR fluorescence imaging system optimized for large animal surgery consisting of a 785 nm diode laser as an excitation light source, wide zoom lens (Nikon; Nikon Vision Co., Ltd., Tokyo, Japan) equipped with an 835/45 emission filter, a CCD camera (Orca R2; Hamamatsu Photonics), and control cabinet, designed and built in our laboratory (Figure S6). One pig was used in one experiment, and the experiment was repeated five times (n = 5). After imaging, the lymph nodes were dissected and fixed by 4% formaldehyde. For histological study, fixed lymph node was embedded in Tissue-Tek OCT compound, snap-frozen, and

cryo-sectioned at 8 μm. Sections were stained with H&E or DAPI and were examined by fluorescence microscopy and a DeltaVision PD Restoration Microscope System.

Statistical Analysis. All results are expressed as mean differences and were tested for significance by Student's *t* test, with $p < 0.05$ considered a significant difference.

Conflict of Interest: The authors declare no competing financial interest.

Acknowledgment. The authors acknowledge the financial support from the National Research Foundation of Korea (NRF) grant funded by the Korean government (MEST) (No. 2010-0026793 and 2009, University-Institute Cooperation Program), the National Research Facilities & Equipment Centre grant, the National Agenda Project grant from Korea Research Council of Fundamental Science and Technology, and the Korea Health Technology R&D Project, Ministry of Health & Welfare (No. A111918).

Supporting Information Available: Synthetic scheme, chemical structure, and detailed characterization data of NIR-PNG nanoprobes are provided. This material is available free of charge *via* the Internet at http://pubs.acs.org.

REFERENCES AND NOTES

1. Morton, D. L.; Wen, D. R.; Wong, J. H.; Economou, J. S.; Cagle, L. A.; Storm, F. K.; Foshag, L. J.; Cochran, A. J. Technical Details of Intraoperative Lymphatic Mapping for Early Stage Melanoma. *Arch. Surg.* **1992**, *127*, 392–399.
2. Kim, S.; Lim, Y. T.; Soltesz, E. G.; De Grand, A. M.; Lee, J.; Nakayama, A.; Parker, J. A.; Mihaljevic, T.; Laurence, R. G.; Dor, D. M.; *et al*. Near-Infrared Fluorescent Type II Quantum Dots for Sentinel Lymph Node Mapping. *Nat. Biotechnol.* **2004**, *22*, 93–97.
3. Soltesz, E. G.; Kim, S.; Laurence, R. G.; DeGrand, A. M.; Parungo, C. P.; Dor, D. M.; Cohn, L. H.; Bawendi, M. G.; Frangioni, J. V.; Mihaljevic, T. Intraoperative Sentinel Lymph Node Mapping of the Lung Using Near-Infrared Fluorescent Quantum Dots. *Ann. Thorac. Surg.* **2005**, *79*, 269–277.
4. Takeuchi, H.; Kitajima, M.; Kitagawa, Y. Sentinel Lymph Node as a Target of Molecular Diagnosis of Lymphatic Micrometastasis and Local Immunoresponse to Malignant Cells. *Cancer Sci.* **2008**, *99*, 441–450.
5. Hayashi, H.; Ochiai, T.; Mori, M.; Karube, T.; Suzuki, T.; Gunji, Y.; Hori, S.; Akutsu, N.; Matsubara, H.; Shimada, H. Sentinel Lymph Node Mapping for Gastric Cancer Using a Dual Procedure with Dye- and Gamma Probe-Guided Techniques. *J. Am. Coll. Surg.* **2003**, *196*, 68–74.
6. Saha, S.; Sehgal, R.; Patel, M.; Doan, K.; Dan, A.; Bilchik, A.; Beutler, T.; Wiese, D.; Bassily, N.; Yee, C. A Multicenter Trial of Sentinel Lymph Node Mapping in Colorectal Cancer: Prognostic Implications for Nodal Staging and Recurrence. *Am. J. Surg.* **2006**, *191*, 305–310.
7. Park, J. C.; Yu, M. K.; An, G. I.; Park, S. I.; Oh, J.; Kim, H. J.; Kim, J. H.; Wang, E. K.; Hong, I. H.; Ha, Y. S.; *et al*. Facile Preparation of a Hybrid Nanoprobe for Triple-Modality Optical/PET/MR Imaging. *Small* **2010**, *6*, 2863–2868.
8. Kitayama, J.; Ishigami, H.; Ishikawa, M.; Yamashita, H.; Soma, D.; Miyato, H.; Nagawa, H. Hyaluronic Acid Is a Useful Tool for Intraoperative Sentinel Node Detection in Gastric Cancer Surgery. *Surgery* **2007**, *141*, 815–820.
9. Frangioni, J. V. *In Vivo* Near-Infrared Fluorescence Imaging. *Curr. Opin. Chem. Biol.* **2003**, *7*, 626–634.
10. Soltesz, E. G.; Kim, S.; Kim, S. W.; Laurence, R. G.; De Grand, A. M.; Parungo, C. P.; Cohn, L. H.; Bawendi, M. G.; Frangioni, J. V. Sentinel Lymph Node Mapping of the Gastrointestinal Tract by Using Invisible Light. *Ann. Surg. Oncol.* **2006**, *13*, 386–396.
11. Schaafsma, B. E.; Mieog, J. S. D.; Hutteman, M.; Van der Vorst, J. R.; Kuppen, P. J. K.; Lowik, C. W. G. M.; Frangioni, J. V.; Van de Velde, C. J. H.; Vahrmeijer, A. L. The Clinical Use of Indocyanine Green as a Near-Infrared Fluorescent Contrast Agent for Image-Guided Oncologic Surgery. *J. Surg. Oncol.* **2011**, *104*, 323–332.
12. Yang, J.; Choi, J.; Bang, D.; Kim, E.; Lim, E. K.; Park, H.; Suh, J. S.; Lee, K.; Yoo, K. H.; Kim, E. K.; *et al*. Convertible Organic Nanoparticles for Near-Infrared Photothermal Ablation of Cancer Cells. *Angew. Chem., Int. Ed.* **2011**, *50*, 441–444.
13. Noh, Y. W.; Park, H. S.; Sung, M. H.; Lim, Y. T. Enhancement of the Photostability and Retention Time of Indocyanine Green in Sentinel Lymph Node Mapping by Anionic Polyelectrolytes. *Biomaterials* **2011**, *32*, 6551–6557.
14. Yoshida, M.; Kubota, K.; Kuroda, J.; Ohta, K.; Nakamura, T.; Saito, J.; Kobayashi, M.; Sato, T.; Beck, Y.; Kitagawa, Y.; Kitajima, M. Indocyanine Green Injection for Detecting Sentinel Nodes Using Color Fluorescence Camera in the Laparoscopy-Assisted Gastrectomy. *J. Gastroenterol. Hepatol.* **2012**, *27*, 29–33.
15. Ohnishi, S.; Lomnes, S. J.; Laurence, R. G.; Gogbashian, A.; Mariani, G.; Frangioni, J. V. Organic Alternatives to Quantum Dots for Intraoperative Near-Infrared Fluorescent Sentinel Lymph Node Mapping. *Mol. Imaging* **2005**, *4*, 172–181.
16. Zhang, C.; Wang, S.; Xiao, J.; Tan, X.; Zhu, Y.; Su, Y.; Cheng, T.; Shi, C. Sentinel Lymph Node Mapping by a Near-Infrared Fluorescent Heptamethine Dye. *Biomaterials* **2010**, *31*, 1911–1917.
17. Kitai, T.; Inomoto, T.; Miwa, M.; Shikayama, T. Fluorescence Navigation with Indocyanine Green for Detecting Sentinel Lymph Nodes in Breast Cancer. *Breast Cancer* **2005**, *12*, 211–215.
18. Tajima, Y.; Yamazaki, K.; Masuda, Y.; Kato, M.; Yasuda, D.; Aoki, T.; Kato, T.; Murakami, M.; Miwa, M.; Kusano, M. Sentinel Node Mapping Guided by Indocyanine Green Fluorescence Imaging in Gastric Cancer. *Ann. Surg.* **2009**, *249*, 58–62.
19. Moody, E. D.; Viskari, P. J.; Colyer, C. L. Non-Covalent Labeling of Human Serum Albumin with Indocyanine Green: A Study by Capillary Electrophoresis with Diode Laser-Induced Fluorescence Detection. *J. Chromatogr. B. Biomed. Sci. Appl.* **1999**, *729*, 55–64.
20. Saxena, V.; Sadoqi, M.; Shao, J. Polymeric Nanoparticulate Delivery System for Indocyanine Green: Biodistribution in Healthy Mice. *Int. J. Pharm.* **2006**, *308*, 200–204.
21. Kim, T. H.; Chen, Y.; Mount, C. W.; Gombotz, W. R.; Li, X.; Pun, S. H. Evaluation of Temperature-Sensitive, Indocyanine Green-Encapsulating Micelles for Noninvasive Near-Infrared Tumor Imaging. *Pharm. Res.* **2010**, *27*, 1900–1913.
22. Reddy, S. T.; Rehor, A.; Schmoekel, H. G.; Hubbell, J. A.; Swartz, M. A. *In Vivo* Targeting of Dendritic Cells in Lymph Nodes with Poly(Propylene Sulfide) Nanoparticles. *J. Controlled Release* **2006**, *112*, 26–34.
23. Reddy, S. T.; van der Vlies, A. J.; Simeoni, E.; Angeli, V.; Randolph, G. J.; O'Neill, C. P.; Lee, L. K.; Swartz, M. A.; Hubbell, J. A. Exploiting Lymphatic Transport and Complement Activation in Nanoparticle Vaccines. *Nat. Biotechnol.* **2007**, *25*, 1159–1164.
24. Kim, S. W.; Zimmer, J. P.; Ohnishi, S.; Tracy, J. B.; Frangioni, J. V.; Bawendi, M. G. Engineering InAsxP1-x/InP/ZnSe III-V Alloyed Core/Shell Quantum Dots for the Near-Infrared. *J. Am. Chem. Soc.* **2005**, *12*, 10526–10532.
25. Erogbogbo, F.; Yong, K.-T.; Roy, I.; Hu, R.; Law, W.-C.; Zhao, W.; Ding, H.; Wu, F.; Kumar, R.; Swihart, M. T.; *et al*. *In Vivo* Targeted Cancer Imaging, Sentinel Lymph Node Mapping and Multi-Channel Imaging with Biocompatible Silicon Nanocrystals. *ACS Nano* **2010**, *5*, 413–423.
26. Pons, T.; Pic, E.; Lequeux, N.; Cassette, E.; Bezdetnaya, L.; Guillemin, F. o.; Marchal, F. d. r.; Dubertret, B. Cadmium-Free $CuInS_2$/ZnS Quantum Dots for Sentinel Lymph Node Imaging with Reduced Toxicity. *ACS Nano* **2010**, *4*, 2531–2538.
27. Derfus, A. M.; Chan, W. C. W.; Bhatia, S. N. Probing the Cytotoxicity of Semiconductor Quantum Dots. *Nano Lett.* **2003**, *4*, 11–18.
28. Gokarna, A.; Jin, L. H.; Hwang, J. S.; Cho, Y. H.; Lim, Y. T.; Chung, B. H.; Youn, S. H.; Choi, D. S.; Lim, J. H. Quantum Dot-Based Protein Micro- and Nanoarrays for Detection of Prostate Cancer Biomarkers. *Proteomics* **2008**, *8*, 1809–1818.

29. Bruneel, D.; Schacht, E. Enzymatic Degradation of Pullulan and Pullulan Derivatives. *J. Bioact. Compat. Polym.* **1995**, *10*, 299–312.
30. Cheng, K.-C.; Demirci, A.; Catchmark, J. Pullulan: Biosynthesis, Production, and Applications. *Appl. Microbiol. Biotechnol.* **2011**, *92*, 29–44.
31. Na, K.; Lee, E. S.; Bae, Y. H. Adriamycin Loaded Pullulan Acetate/Sulfonamide Conjugate Nanoparticles Responding to Tumor pH: pH-Dependent Cell Interaction, Internalization and Cytotoxicity *in Vitro*. *J. Controlled Release* **2003**, *87*, 3–13.
32. Hasegawa, U.; Nomura, S. M.; Kaul, S. C.; Hirano, T.; Akiyoshi, K. Nanogel-Quantum Dot Hybrid Nanoparticles for Live Cell Imaging. *Biochem. Biophys. Res. Commun.* **2005**, *331*, 917–921.
33. Suginoshita, Y.; Tabata, Y.; Matsumura, T.; Toda, Y.; Nabeshima, M.; Moriyasu, F.; Ikada, Y.; Chiba, T. Liver Targeting of Human Interferon-β with Pullulan Based on Metal Coordination. *J. Controlled Release* **2002**, *83*, 75–88.
34. Zhuang, X.; Ha, T.; Kim, H. D.; Centner, T.; Labeit, S.; Chu, S. Fluorescence Quenching: A Tool for Single-Molecule Protein-Folding Study. *Proc. Natl. Acad. Sci. U. S. A.* **2000**, *97*), 14241–14244.
35. Thevarajah, S.; Huston, T. L.; Simmons, R. M. A Comparison of the Adverse Reactions Associated with Isosulfan Blue *versus* Methylene Blue Dye in Sentinel Lymph Node Biopsy for Breast Cancer. *Am. J. Surg.* **2005**, *189*, 236–239.